Original article

Chaitra Venkatesh, Yuanyuan Chen, Zhi Cao, Shane Brennan, Ian Major, John G. Lyons and Declan M. Devine*

Influence of extrusion screw speed on the properties of halloysite nanotube impregnated polylactic acid nanocomposites

https://doi.org/10.1515/polyeng-2020-0228
Received September 3, 2020; accepted April 8, 2021;
published online ■■■

Abstract: Poly (lactic acid)/halloysite nanotube (PLA/HNT) nanocomposites have been studied extensively over the past few years owing to the interesting properties of the polymer, PLA, and the nanoclay, HNT, individually and as composites. In this paper, the influence of the screw speed during extrusion was investigated and was found to have a significant impact on the mechanical and thermal performance of the extruded PLA/HNT nanocomposites. To determine the effect of screw speed on PLA/HNT nanocomposites, 5 and 10 wt% of HNTs were blended into the PLA matrix through compounding at screw speeds of 40, 80, and 140 rpm. Virgin PLA was compounded for comparison. The resultant polymer melt was quench cooled onto a calendar system to produce composite films which were assessed for mechanical, thermal, chemical, and surface properties. Results illustrate that in comparison to 40 and 80 rpm, the virgin PLA when compounded at 140 rpm, indicated a significant increase in the mechanical properties. The PLA/HNT 5 wt% nanocomposite compounded at 140 rpm showed significant improvement in the dispersion of HNTs in the PLA matrix which in turn enhanced the mechanical and thermal properties. This can be attributed to the increased melt shear at higher screw speeds.

Keywords: biodegradable; halloysite nanotubes; nanocomposites; poly (lactic acid); twin-screw extrusion.

***Corresponding author: Declan M. Devine**, Materials Research Institute, Athlone Institute of Technology, Dublin Road, Athlone, Co. Westmeath, Ireland, E-mail: ddevine@ait.ie. https://orcid.org/0000-0002-1364-5583
Chaitra Venkatesh, Yuanyuan Chen, Zhi Cao, Shane Brennan and Ian Major, Materials Research Institute, Athlone Institute of Technology, Dublin Road, Athlone, Co. Westmeath, Ireland. https://orcid.org/0000-0003-4105-6273 (C. Venkatesh)
John G. Lyons, Faculty of Engineering and Informatics, Athlone Institute of Technology, Dublin Road, Athlone, Co. Westmeath, Ireland

1 Introduction

Biodegradable polymers derived from renewable sources have been of great research interest over the past decade as they solve the problems of waste disposal of petroleum-based thermoplastics [1–4]. Biodegradable polymers have been used in various biomedical applications such as sutures, tissue engineering, etc. [5]. However, on its own, it cannot meet all the required properties for some biomedical applications. Therefore, consideration for selection of polymers, incorporation of nanofillers, and processing methods aids to prepare biodegradable polymer nanocomposites with improved properties for biomedical applications [6]. Biodegradable polymer nanocomposites, in which the nanofillers act as a reinforcing agent in the polymer when added in small quantities have been of significant interest because of nanoparticle properties such as high surface reactivity, large surface area, and relatively low cost. Nanofillers improve various polymer properties producing high mechanical strength and thermal resistance in a polymer nanocomposite. The nanomaterial can be reinforced into polymer via solution mixing or extrusion [7–10]. Also, the size of the nanofillers does not produce stress points in the polymer matrix and in turn, does not lead to material failure when dispersed uniformly without agglomeration.

Polylactic acid (PLA) polymer has characteristics such as biodegradability, high mechanical properties, easy availability, and processability [11, 12]. PLA has been researched and used for various medical applications such as resorbable sutures, tissue engineering, drug delivery systems, and dental, ophthalmic, fracture fixation [13, 14]. However, there is a limitation of the use of PLA in many applications due to low crystallinity and extreme brittleness [15]. PLA is commonly blended with clay-based nanofillers to improve the mechanical and thermal properties as the clay nanofiller has good strength on its own with a large aspect ratio [14, 16, 17].

Halloysite nanotubes (HNT) is a type of clay mineral formed naturally in the earth and has a high aspect ratio

(length/diameter), biocompatibility, nontoxicity, and easy availability at low cost [14, 18–20]. Because of these characteristics, they have been researched for biomedical applications such as dental fillers, drug delivery, cosmetics, cancer cell isolation, etc. [21]. HNT has been used as nanofillers for various polymer nanocomposites and has shown to improve the mechanical properties of the composite without the need for surface treatment [22, 23]. They have been studied for easy and uniform dispersion in the polymer matrix such as polyamide and polypropylene by direct melt blending without the need for surface modification of HNT [24, 25].

PLA/HNT nanocomposites are of great interest in the biomedical field owing to the relatively high strength of PLA compared to other biodegradable polymers and the natural, original, and biocompatibility of HNT. It has been shown in earlier studies that 10 wt% HNT loadings result in increases in the mechanical, thermal properties [7, 26–28], and flame retardant properties [7, 29] of PLA. It has further been shown that surface treatment of HNT can be used to improve dispersion of the nanoparticles in the PLA matrix [26, 28, 30]. However, very little research has been done on the influence of screw speeds during extrusion for the PLA/HNT composites.

Melt blending is a method of amalgamating two or more polymers into a single material with blended properties [31] or combining clay and polymer as a nanocomposite for better dispersion with enhanced properties [32]. Twin-screw extrusion is a type of hot-melt extrusion process where the material melts under high temperature in the barrel and continues to move towards the die with a homogenous melt or dispersion [33]. It has been extensively used for various applications such as plastic, food, and pharmaceutical industries [14, 34, 35].

Other research works suggest that the shear force from high screw speed during melt blending improves the dispersion of the nanoclay in the polymer matrix. Li et al. postulated that an increase in shear force during melt blending enhances the dispersion of the clay when they investigated polymer/clay nanocomposites [36]. Sasimowski et al. investigated the extrusion process and showed that the screw speed had a great impact on the efficiency of the extrusion process, the pressure of the processed material, polymer mass flow rate, and the energy consumption of the extruder [37]. Albareeki et al. studied the effect of screw speed on the melt temperature, drive torque, and residence time in the extruder and found that increasing the screw speed increases the melt temperature and there is a decrease in the residence time with better dispersion of the filler in the polymer matrix [38]. Mixing of thermoplastic pellets with carbon nanotube (CNT) in a twin-screw extruder had good dispersion by shear flow created at high screw speed [39]. Thus, to eliminate the need for surface treatment of HNT, in the current study, the processing of PLA/HNT was examined by varying the screw speed keeping other parameters of extrusion constant throughout.

The present work mainly evaluates the mechanical and thermal properties of the nanocomposites with two mass fractions of 5 and 10 wt% of the nanoclay HNT blended into the PLA matrix using a twin-screw extruder with three different screw speeds of 40, 80, and 140 rpm based on findings in previous work where a low screw speed resulted in poor HNT dispersion without surface modification [28]. The nanocomposite produced is characterized by tensile testing, differential scanning calorimetry (DSC), dynamic mechanical analysis (DMA), scanning electron microscopy (SEM), Fourier transform infrared microscopy, and surface wettability.

2 Materials and methods

2.1 Materials

PLA was obtained from Corbion, PLA LX 175 (Total Corbian, Gorinchem, The Netherlands). The density of the PLA is 1.24 g/cm^3, melting temperature of 155 °C, and glass transition temperature of 55–60 °C. HNT was supplied by Applied Minerals; DRAGONITE-HP (APPLIED MINERALS INC, Brooklyn, NY, USA) and had a density of 2.56 g/cm^3, length of 0.2–2.0 μm, and aspect ratio (L/D) of 10–20. All materials were dried before use. PLA was dried at 80 °C for 4 h and HNT was dried at 100 °C for 3 h.

2.2 Processing

Extrusion was performed by using APV (Model MP19TC (25:1)), APV Baker, Newcastle-under-Lyme, UK) twin-screw compounder with 19 mm diameter screws and length-diameter ratio *L/D* of 25/1. The temperature profile was maintained at (from die to the feeder) 200/190/180/170/160/110/50 °C. The feed rate and barrel temperature were kept constant throughout. Three different screw speeds were selected for the study: 40, 80, and 140 rpm. The different mass fractions of 100:0, 95:5, and 90:10 for PLA: HNT were prepared for extrusion by tumble mixing of the dried PLA pellets with the dried HNT powder in a container and fed into the hopper of the extruder.

Extruded films of the molten composite were then drawn through a three-roll calendar. Cooling of the calendar rolls and extruder barrel was provided by a constant flow of tap water temperature (ca. 12 °C). Similarly, the virgin PLA was processed by melt compounding under similar conditions for comparison. These samples were punched out from the center of the film into ASTM International standard tensile test specimen with a sample cutter using a physical punching process.

2.3 Differential scanning calorimetry

DSC was conducted out using a DSC 2920 Modulated DSC (TA Instruments, New Castle, DE, USA). To prevent oxidation, a nitrogen

flow rate of 20 mL/min was applied. Indium was used as a standard to calibrate the instrument. Test specimens were weighed on a Sartorius scale (MC 210 P, Sartorius Lab Instruments GmbH & Co. KG, Goettingen, Germany) measuring between 8 and 12 mg. Samples were crimped in nonperforated aluminum pans, with an empty crimped aluminum pan used as the reference. The thermal history was removed by heating samples from 20–220 °C at the rate of 30 °C/min and then held isothermally at 220 °C for 10 min. The samples were then cooled down from 220–20 °C at 30 °C/min. Finally, the thermal properties of the samples were recorded by heating the samples from 20–220 °C at the rate of 10 °C/min, glass transition temperature, and melting temperature of each sample was recorded.

2.4 Tensile testing

Mechanical properties of the PLA/HNT composites were characterized by tensile testing each different blend. Tensile testing was carried out on a Lloyd Lr10k tensometer (Ametek Ltd, West Sussex, UK) using a 2.5 kN load cell on ASTM standard test specimens at a strain rate of 50 mm/min. Data were recorded using Nexygen™ software (Ametek ltd). The tensile tests were carried out in adherence to ASTM D 882. Ten individual test specimens were analyzed per batch and the thickness of each sample was measured before testing. The percentage strain at maximum load, stress at maximum load, stiffness, and Young's modulus of each tested sample were recorded.

2.5 Scanning electron microscopy

SEM was performed using a Mira XMU SEM (TESCAN Brno, Czech Republic) in a backscattered electron mode to determine the shape and distribution of HNTs in the PLA matrix. Energy Dispersive X-ray (EDX) was performed using an Oxford Instruments detector to determine the elemental composition of HNT and the composites of PLA and HNT. The accelerating voltage utilized was 10 kV for raw HNT and 20 kV for composite materials. Before analysis, test samples were placed on an aluminum stub and the samples were sputtered with gold using Baltec SCD 005 for 110 s at 0.1 mbar vacuum before testing.

2.6 Fourier transform infrared spectroscopy

Fourier transform infrared spectroscopy (FTIR) was carried out on a Perkin Elmer Spectrum One fitted with a universal ATR sampling accessory (Perkin Elmer, Waltham, MA, USA). All data were recorded in the spectral range of 4,000–650 cm^{-1} and at 21 °C. A fixed universal compression force of 70–80 N was utilized and each sample was recorded with four scans. Following analysis of the recordings was carried out using Spectrum software.

2.7 Contact angle (goniometry)

The prepared nanocomposites were assessed for the surface wettability properties by using First 10 Angstrom's, FTA32 goniometer (FTA Europe, Cambridge, UK). In this test, the Sessile Drop contact angle technique was utilized and distilled water was used as the probe liquid. Five total measurements at various places on the films were taken for each sample.

2.8 Dynamic mechanical analysis

DMA was used to measure storage modulus, loss modulus, and loss factor (tan delta) and were determined using TA Instrument Q800 DMA (TA Instruments, Eschborn Germany). A strain frequency of 1 Hz and 20 μm amplitude was used. The heating ramp from ambient temperature to 120 °C was carried out at a rate of 3 °C/min.

2.9 Statistical analysis

Statistical analysis of the tensile test results, DSC measurements, and the void content measurements were carried out using General Linear Model of two-way Analysis of variance (ANOVA) in Minitab 17 Statistical Software (Minitab Ltd., Coventry, UK). All the values were considered at a 95% confidence interval and p-values are considered significant when $p \leq 0.05$.

3 Results and discussion

3.1 Processing of PLA and HNT through melt blending

The compounded PLA and PLA/HNT nanocomposites remained transparent in color, however, the nanocomposite changed in color from transparent to opaque with the blending of HNT at all the different screw speeds. This color change could be attributed to the nucleating effect of HNT in the PLA matrix which was similarly observed by De Silva et al. [27]. This was also observed by Liu et al. with injection-molded composite of PLA and HNT [40] and by Chen et al. with extruded PLA/HNT composite [41].

The screw configuration used is illustrated in Figure 1. It had a feeding zone followed by a mixing section comprising two sets of kneading block elements. The first kneading set had 10 paddles, four of which had a forwarding angle of 30°, 60° for the next six, and the remaining paddle at 90°. The second block near the discharge end had six paddles with a 60° forwarding angle. The end of the screw had a metering zone of conveying elements. Processing parameters were varied only in terms of screw speed, which in turn reduces the residence time in general which was in the range of 1–3 min.

Twin-screw extrusion is a high shear process, which aids dispersion of different components during melt processing. The main focus of this study was to assess the effect of screw speeds as increases in screw speed during compounding have been shown to increase melt shear and as such homogeneity of the final compounded material. Gamon et al. hypothesized that a screw speed of 150 rpm was ideal to obtain homogenous properties of fiber-reinforced PLA composites [42]. Normand et al. demonstrated that when the screw speed is increased from 100 to

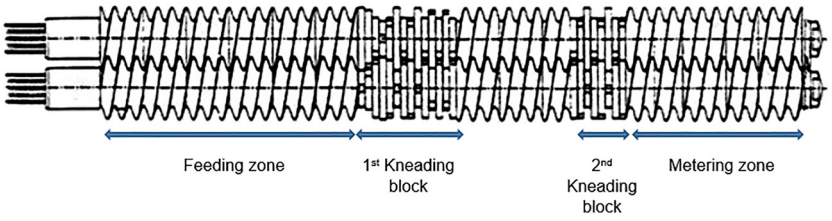

Figure 1: Schematic representation of the screw profile geometry.

600 rpm while compounding polypropylene/clay nanocomposites, the number of the agglomerates decreases and screw speeds higher than 600 rpm did not improve the state of the microscopic dispersion nor had better exfoliation which could be due to the thermal degradation of the clay modifier, mechanical breakage of the clay sheets, or degradation of the matrix [43]. Similarly, Domenech et al. found a reduction in the size of the clay agglomerate as the screw speed increases principally between 100 and 500 rpm. And more than 500 rpm did not show any changes [44]. Conversely, previous work by Chen et al. showed that screw speeds of 35 rpm did not give sufficient mixing and necessitated the surface treatment of HNT to improve dispersion [28]. Hence, in this study, the polymer PLA and the PLA/HNT nanocomposites were compounded at three screw speeds of 40, 80, and 140 rpm for comparison. Higher screw speeds could lead to thermal degradation of the nanocomposite. However, the selected screw speeds were not exhaustive and the effects of dispersion at higher screw speeds cannot be assumed based on these findings.

The filler dispersion and melt blending are augmented and intensified by the kneading elements of the screw configuration [45]. Thus, using the above-described screw configuration with two kneading elements in the mixing section, three different screw speeds were investigated.

3.2 Differential scanning calorimetry

The compounded polymer and the nanocomposites were analyzed for the influence of screw speed on the thermal properties by DSC. The DSC curves show that the addition of HNT into the PLA matrix with different loadings and compounding at different screw speeds showed no significant difference in the glass transition temperature (T_g) with $p = 0.42$ as shown in Table 1 and Figure 2. A similar result has been reported previously [29].

As seen in Table 1, the cold crystallization temperature (T_{cc}) decreases compared to PLA. With $p = 0.00$, the statistical analysis confirmed the decrease with an effect of both HNT loading and screw speed. The decrease in the T_{cc} indicated that HNT has a nucleating effect on the PLA [40, 46] and that heterogeneous nucleation was likely to occur where thinner crystalline lamella was formed compared to that of virgin PLA [26]. Hence, the melting temperature of the composite was also lower than that of virgin PLA. A similar decrease in cold crystallization temperature and the melting temperature was observed by Prashanta et al. Chen et al., Wu et al., and Guo et al. in their study using surface-treated HNT [28, 30, 46, 47].

Table 1: Values corresponding to the glass transition (T_g), cold crystallization temperature (T_{cc}), melting temperature (T_m) of the secondary heating DSC curves, and the tan δ peaks of the dynamic mechanical analysis for the PLA/HNT nanocomposites.

RPM	Loading	T_g	T_{cc}	T_m (first peak)	T_m (second peak)	Tan δ
40	PLA0	60.74	128.22	159.3	0	66.61
40	PLA/HNT5	61.07	117.04	150.15	155.79	64.58
40	PLA/HNT10	60.67	118.36	150.5	155.17	65.56
80	PLA0	62.32	118.92	151.29	0	63.59
80	PLA/HNT5	62.43	118.70	150.44	155	63.87
80	PLA/HNT10	61.31	116.52	149.95	154.91	65.02
140	PLA0	61.21	125.68	157.37	0	62.73
140	PLA/HNT5	60.25	118.14	150.57	155.11	67.47
140	PLA/HNT10	60.69	116.20	149.74	156.2	63.46

A single melting peak was observed for virgin PLA. However, a secondary melting peak was observed for 5 wt % and becomes clearer for 10 wt% loading of the HNT when compounded as 140 rpm as seen in Figure 2. This was observed in other studies by Chen et al. [28] and Prashantha et al. [47] who reported that this was due to the melting of the crystals formed in the cold crystallization stage during heating and followed by recrystallization and further melting processes at higher temperatures [47]. Statistical analysis confirmed the above results with $p = 0.06$ for T_m, the percentage loading of the HNT affected the decrease of T_m.

3.3 Dynamic mechanical analysis

The DMA was used to evaluate the viscoelastic properties of the PLA/HNT nanocomposite below and above the

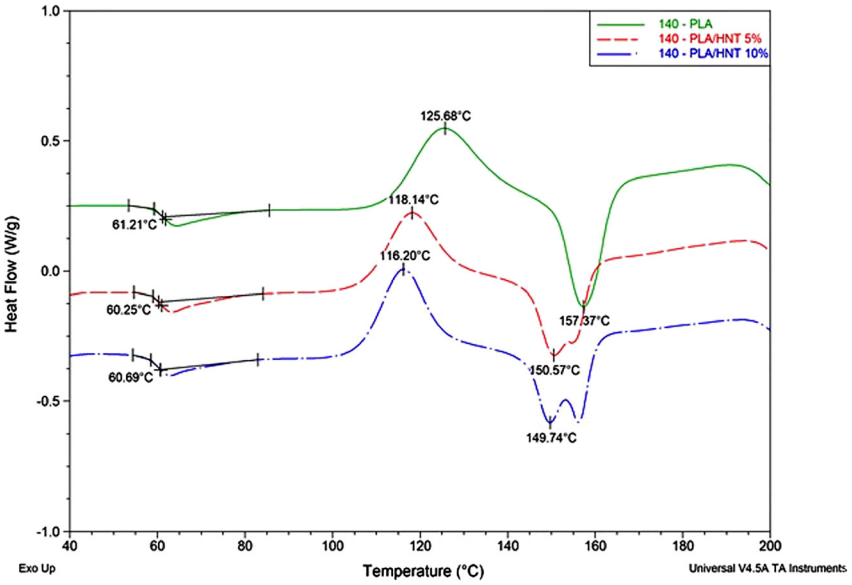

Figure 2: Secondary heating DSC curves for the virgin PLA and PLA/HNT nanocomposites for 140 rpm screw speed. The peak maximum for the glass transition, cold crystallization, and melting temperature are shown.

glass transition. The temperature at the peak of the tan δ curve was considered as the T_g of the material. The tan δ peaks as listed in Table 1 show no significant difference in T_g. The glass transition temperature T_g is a measure of rigidity [48] and the T_g does not show any considerable difference from the DSC results. However, the analysis of T_g is more accurately determined by DMA [40]. Hence, the results from the DMA were statistically analyzed to confirm that there is no significant difference in T_g with an increase in screw speed.

3.4 Mechanical properties

Mechanical testing results found that the Young's modulus increased significantly ($p = 0.02$) with the increase in screw speed for both virgin PLA and the nanocomposites as shown in Figure 3. There is a significant increase in the Young's modulus for the virgin PLA at 140 rpm screw speed when compared to 40 and 80 rpm screw speeds separately. The Young's modulus for the composite increases with an increase in screw speed. However, 10 wt% HNT loaded nanocomposite compounded at 140 rpm screw speed is at maximum. Hence, the screw speed and the percentage loadings of the HNT have a significant effect on the Young's modulus of the composite.

The tensile strength of the material compounded at 140 rpm screw speed significantly increases with $p = 0.039$. It should be noted that the highest tensile strength is for 5 wt% HNT loaded nanocomposite at 140 rpm screw speed. The stiffness of the virgin PLA and the 10 wt% loaded HNT composite significantly increases when compounded at 140 rpm screw speed. However, the elongation at break is significantly increased for virgin PLA and the 5 wt% composites at higher screw speed. Statistical analysis confirms both the screw speed and the loadings of HNT had a significant effect with the p-value = 0.01 on the stiffness and the elongation at break.

Compounding at 140 rpm screw speed improved the mechanical properties of the composites. It is noteworthy that the mechanical properties improve significantly for virgin PLA itself as the screw speed increases. This could be attributed to the high shear force at higher screw speed when the polymer structure rearranges during the extrusion process. It is noticed that the Young's modulus and the stiffness increase for 10 wt% HNT loaded composites. Additionally, the tensile strength and the elongation at break increases by 5 wt% HNT loaded composites for 140 rpm screw speed. The improvement in the tensile strength usually indicates good interfacial bonding resulting in effective stress transfer from the PLA matrix to the reinforcing nanoclay. Guo et al. reported similar improvements when processed by mini extruder at 50 rpm when utilizing surface-modified HNT [30]. Hence, we can say that melt compounding at 140 rpm or higher screw speed had equivalent results without the modification of HNT.

3.5 Morphology and structural characteristics

SEM photomicrographs indicated that the structure of the PLA was uniform, and its elemental composition as measured by EDX was recorded with only carbon and

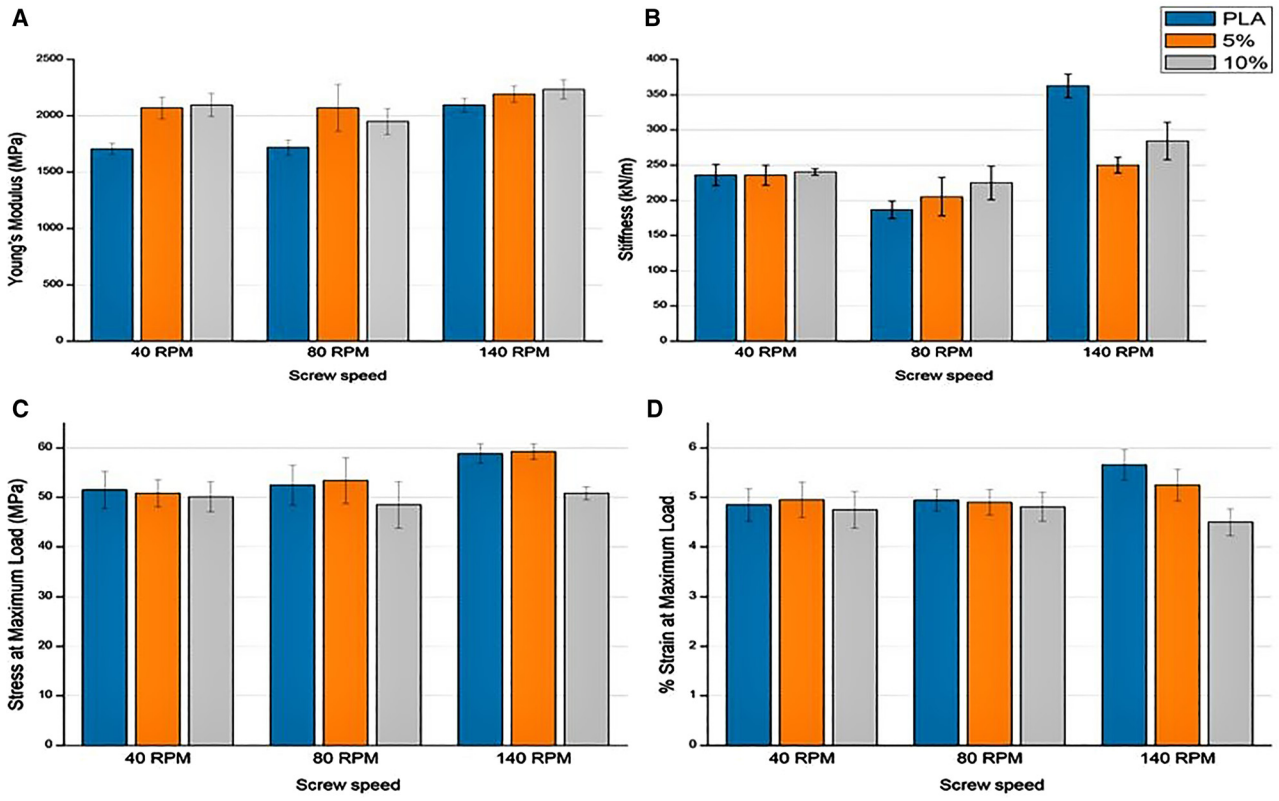

Figure 3: Increased screw speed and HNTs loadings had a significantly:
(A) increased Young's modulus of PLA and PLA/HNTs composites ($p = 0.02$); (B) increased stiffness for virgin PLA and the 10 wt% nanocomposites ($p = 0.01$). Increased screw speed; (C) increased tensile strength of PLA and 5 wt% PLA/HNTs composites ($p = 0.039$); (D) and increased elongation for PLA while decreasing it for PLA/HNTs composites ($p = 0.01$).

oxygen. The incorporation of HNT resulted in the presence of microscale particles, which exhibited an elemental composition consisting of aluminum and silicon which is indicative of the presence of HNT. The heterogeneous structure is observed for 10 wt% loadings of HNT for all screw speeds. This is due to the presence of agglomerates of HNT with the magnitude of the agglomerates being larger in the 10 wt% composites. The magnified image of the agglomerate size on the 10 wt% composite in Figure 4D indicates the cluster of HNT for a wide area. Furthermore, very few agglomerations of small sizes were apparent in 5 wt% composites compounded at 140 rpm as seen in Figure 4B could indicate a better distribution of HNT in the matrix.

The elemental composition of the composite as seen in Table 2 indicated the presence of aluminum and silicone from the composition of the HNT, which confirmed the presence of HNT in the polymer matrix. In some, there was an agglomeration of HNT and spaces between the particles and the matrix. From Table 2 and Figure 4, the dispersion of HNT into the polymer matrix appears to increase with the increase in screw speed by the increase in the amount of aluminum and silicone present which are elemental in the composition of the HNT.

3.6 Fourier transfer infrared spectroscopy

FTIR spectra for PLA, HNT, and PLA/HNT composites are shown in Figure 5. Virgin PLA exhibited characteristic absorption band at 3571 cm^{-1} corresponding to –OH stretch and absorption bands at 2996 and 2946 cm^{-1} are attributed to CH stretch and the absorption band at 1750 cm^{-1} corresponding to –C=O carbonyl group [11]. The characteristic absorption band at 1450 cm^{-1} is attributed to the bending vibrations of CH_3 and absorption bands at 1384 and 1364 cm^{-1} are the CH deformation and asymmetric/symmetric bending [40]. The spectrum of HNT displayed absorption bands at 3695 and 3621 cm^{-1} that can be assigned to O–H group vibrations and absorption band at 910 cm^{-1} to Al–OH group vibrations.

The spectra of PLA/HNT composites revealed the absorption bands of both PLA and HNT. The overlapping of

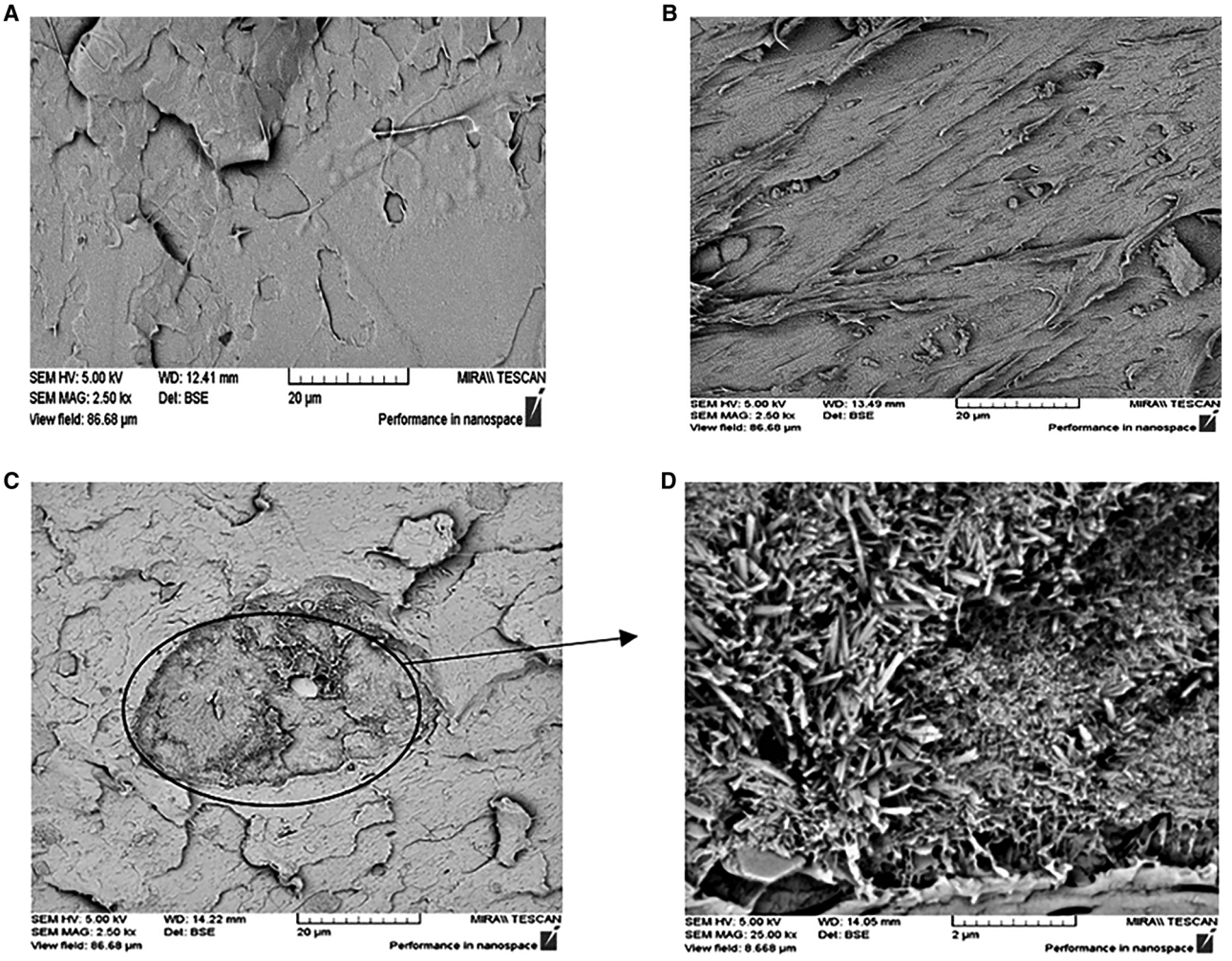

Figure 4: SEM photomicrograph of the surface topography of PLA and PLA/HNT nanocomposites.
(A) PLA, (B) 5 wt% composite at 140 rpm, (C) 10 wt% composite at 140 rpm, (D) magnified image of the agglomerate site of the 10 wt% composite where the HNTs are seen.

Table 2: Values corresponding to the elemental composition of aluminum and silicone by EDX.

Sample_screw speed	Aluminum (wt%)	Silicone (wt%)	Sample_screw speed	Aluminum (wt%)	Silicone (wt%)
PLA/HNT5_40	0.43	0.43	PLA/HNT10_40	1.32	1.33
PLA/HNT5_80	0.64	0.66	PLA/HNT10_80	1.82	1.95
PLA/HNT5_140	0.87	0.70	PLA/HNT10_140	1.92	1.98

HNT absorption bands increases the intensity of the PLA absorption band as the screw speed increases in the region between 1300–500 cm^{-1}. For instance, the overlapping of the HNT absorption band 1031 cm^{-1} increases the intensity of the 1043 cm^{-1} absorption band of PLA. This observation is also seen in other studies as well [27, 30, 40]. The absorption band 1266 cm^{-1} of PLA shifts to 1270 cm^{-1} for 5 wt% composites and is more intense and sharpens as the screw speed increases. This kind of shift is also seen in the study by Dong et al. in which the HNT was modified [26]. The observed sharpening, increase in the intensity of the peaks, and shifting to higher frequencies as the screw speed increases are the most for PLA/HNT 5 wt% nanocomposites at 140 rpm. This can be attributed to the interactions

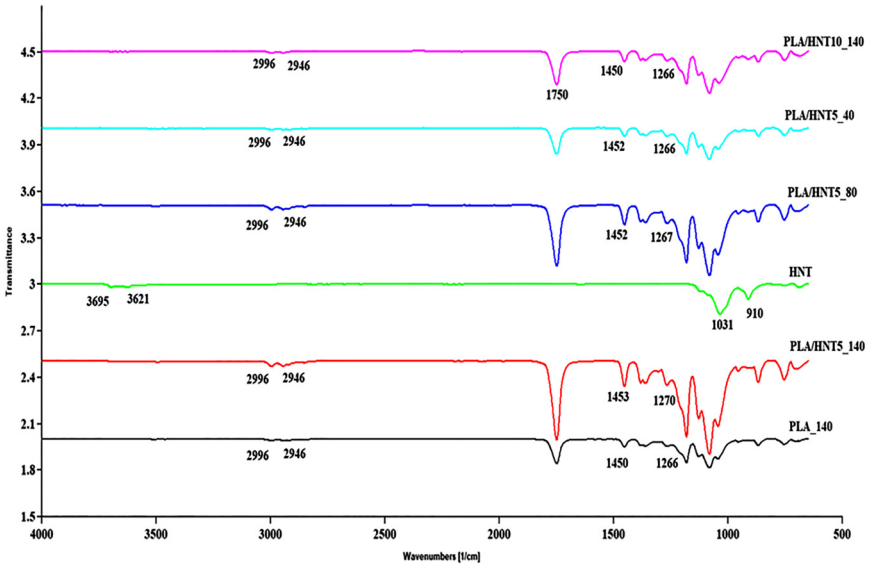

Figure 5: FTIR spectra of HNT, PLA, and PLA/HNT composites at 140 rpm screw speed.

between the PLA and HNT via hydrogen bonding which could have contributed to the increased thermal and mechanical properties of the PLA/HNT composite, which were also confirmed by FTIR in other studies [40].

3.7 Surface wettability

Contact angle measurements for PLA were within a range of 60°–65°. The nanocomposite produced by the incorporation of 5 wt% HNT compounded at different screw speeds did not have a statistically significant effect on the surface wettability of the PLA for $p = 0.245$ and the contact angle remained within the same range as virgin PLA as seen in Figure 6. Hence, they are hydrophilic. However, for 10 wt% composites the contact angle increased to 99° making it hydrophobic.

The contact angle measuring less than 90° corresponds to high wettability and the contact angle more than 90° corresponds to low wettability [49]. The surface of PLA and 5 wt% composite formed at all screw speeds were found to be hydrophilic, which was also seen in the study by De Silva et al. [27]. The 10 wt% composites are hydrophobic as the contact angle increases to greater than 90°. Similar findings have been reported by De Silva et al. which can be attributed to the increase in the surface roughness at higher concentrations. This in turn reduces the surface energy because of more polar groups at higher concentrations of HNT, which makes the material hydrophobic [27].

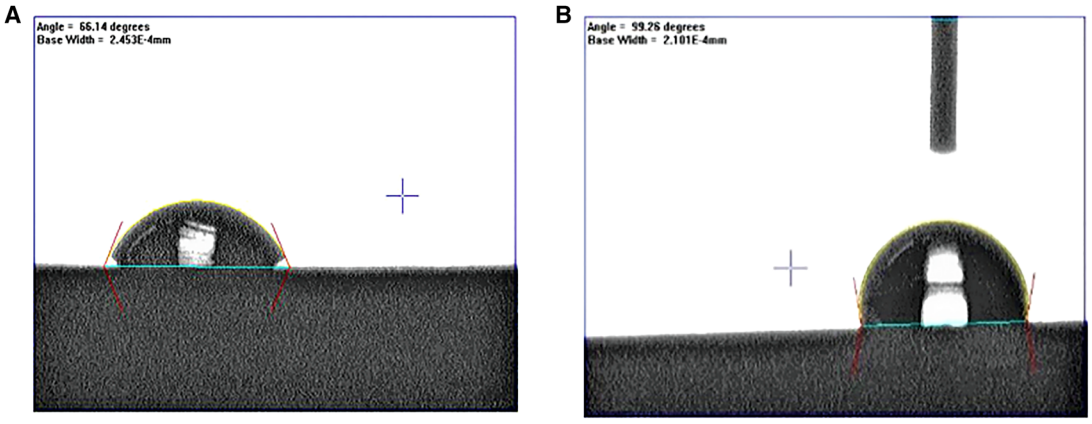

Figure 6: The contact angle of the distilled water on the (A) PLA, PLA/HNT 5 wt% nanocomposite (angle is <90°), (B) PLA/HNT 10 wt% nanocomposite (angle is >90°). The PLA and 5 wt% composite is hydrophilic and 10 wt% composite is hydrophobic.

4 Conclusions

The study of screw speeds during extrusion revealed that compounding at higher screw speed had a significant effect on the HNT loaded composite. This can be attributed to the high melt shear during compounding which enhanced HNT dispersion. The thermal and mechanical properties along with the morphology of the nanocomposites compounded at higher screw speed had at least equivalent results to those reported in the literature where the HNT were surface treated. Hence, we can say that the high melt shear during compounding assists the better dispersion of the HNT into the polymer matrix which in turn improved the overall properties of the composites without the need for surface treatment of the HNT as desired for various biomedical applications. The main focus of the study was to look at the effect of screw speed as we had observed poor HNT dispersion in previous work when processed at low speed. Nevertheless, the combination of screw elements determining the filling degree, melting degree, residence time distributions, or mechanical energy does warrant further investigation.

Author contributions: All the authors have accepted responsibility for the entire content of this submitted manuscript and approved submission.

Research funding: Athlone Institute of Technology under the Presidents Seed Fund, Enterprise Ireland funding under the Technology Gateway program, grant number TG-2017-0114, and Science Foundation Ireland (SFI) under grant number 16/RC/3918.

Conflict of interest statement: The authors declare no conflicts of interest regarding this article.

References

1. Lim L.-T., Auras R., Rubino M. Processing technologies for poly(lactic acid). *Prog. Polym. Sci.* 2008, *33*, 820–852.
2. La Mantia F. P., Morreale M. Green composites: a brief review. *Compos. Part A Appl. Sci. Manuf.* 2011, *42*, 579–588.
3. Rasal R. M., Janorkar A. V., Hirt D. E. Poly(lactic acid) modifications. *Prog. Polym. Sci.* 2010, *35*, 338–356.
4. Lasprilla A. J. R., Martinez G. A. R., Lunelli B. H., Jardini A. L., Filho R. M. Poly-lactic acid synthesis for application in biomedical devices – a review. *Biotechnol. Adv.* 2012, *30*, 321–328.
5. Kunduru K. R., Basu A., Domb A. J. Biodegradable polymers: medical applications. *Encycl. Polym. Sci. Technol.* 2016, 1–22. https://doi.org/10.1002/0471440264.pst027.pub2.
6. Bari S. S., Chatterjee A., Mishra S. Biodegradable polymer nanocomposites: an overview. *Polym. Rev.* 2016, *56*, 287–328.
7. Liu M., Jia Z., Jia D., Zhou C. Recent advance in research on halloysite nanotubes-polymer nanocomposite. *Prog. Polym. Sci.* 2014, *39*, 1498–1525.
8. Anand Narayanan A. G., Babu R., Vasanthakumari R. Studies on halloysite nanotubes (HNT) natural rubber nanocomposites for mechanical thermal and wear properties. *Int. J. Eng. Res. Technol.* 2016, *5*, 152–156.
9. Pollack S., Venkatesh C., Neff M., Healy A. V., Hu G., Fuenmayor E. A., Lyons J. G., Major I., Devine D. M. Polymer-based additive manufacturing: historical developments, process types, and material considerations. In *Polymer-Based Additive Manufacturing*; Devine D., Ed.; Springer Nature Switzerland AG: Switzerland, 2019; pp. 1–22.
10. Venkatesh C., Fuenmayor E., Doran P., Major I., Lyons J. G., Devine D. M. Additive manufacturing of PLA/HNT for biomedical applications. *Procedia Manuf.* 2020, *38*, 17–24.
11. Garlotta D. A literature review of poly (lactic acid). *J. Polym. Environ.* 2002, *9*, 63–84.
12. Chen Y., Geever L. M., Killion J. A., Lyons J. G., Higginbotham C. L., Devine D. M. A review of multifarious applications of poly (lactic acid). *Polym. Plast. Technol. Eng.* 2016, *2559*, 1057–1075.
13. Ramot Y., Haim-Zada M., Domb A. J., Nyska A. Biocompatibility and safety of PLA and its copolymers. *Adv. Drug Deliv. Rev.* 2016, *107*, 153–162.
14. Venkatesh C., Clear O., Major I., Lyons J. G., Devine D. M. Faster release of lumen-loaded drugs than matrix-loaded equivalent in polylactic acid/halloysite nanotubes. *Materials* 2019, *12*, 1830.
15. Dillon B., Doran P., Fuenmayor E., Healy A. V., Gately N. M., Major I., Lyons J. G. Influence of annealing and biaxial expansion on the properties of poly(l-lactic acid) medical tubing. *Polymers* 2019, *11*, 1172.
16. Jia S., Yu D., Zhu Y., Wang Z., Chen L., Fu L. Morphology, crystallization and thermal behaviors of PLA-based composites: wonderful effects of hybrid GO/PEG via dynamic impregnating. *Polymers* 2017, *9*, 528.
17. Sangeetha V. H., Deka H., Varghese T. O., Nayak S. K. State of the art and future prospectives of poly(lactic acid) based blends and composites. *Polym. Compos.* 2018, *39*, 81–101.
18. Lazzara G., Massaro M., Milioto S., Riela S. Halloysite-based bionanocomposites. *Handb. Compos. Renew. Mater.* 2017, *1–8*, 557–584.
19. Yang Y. Recent advances on surface modification of halloysite nanotubes for multifunctional applications. *Appl. Sci.* 2017, *7*, 1215.
20. Kamble R., Ghag M., Gaikwad S., Panda B. K. Review article halloysite nanotubes and applications: a review. *J. Adv. Sci. Res.* 2012, *3*, 25–29.
21. Lvov Y., Abdullayev E. Functional polymer-clay nanotube composites with sustained release of chemical agents. *Prog. Polym. Sci.* 2013, *38*, 1690–1719.
22. Therias S., Murariu M., Dubois P. Bionanocomposites based on PLA and halloysite nanotubes: from key properties to photooxidative degradation. *Polym. Degrad. Stabil.* 2017, *145*, 1–10.
23. Jock Churchman G., Pasbakhsh P., Hillier S. The rise and rise of halloysite. *Clay Miner.* 2016, *51*, 303–308.
24. Du M., Guo B., Jia D. Newly emerging applications of halloysite nanotubes: a review. *Polym. Int.* 2010, *59*, 574–582.

25. Deepak R., Agrawal Y. K. Study of nanocomposites with emphasis to halloysite nanotubes. *Rev. Adv. Mater. Sci.* 2012, *32*, 149–157.
26. Dong Y., Marshall J., Haroosh H. J., Mohammadzadehmoghadam S., Liu D., Qi X., Lau K. T. Polylactic acid (PLA)/halloysite nanotube (HNT) composite mats: influence of HNT content and modification. *Compos. Part A Appl. Sci. Manuf.* 2015, *76*, 28–36.
27. De Silva R. T., Pasbakhsh P., Goh K. L., Chai S. P., Chen J. Synthesis and characterisation of poly (lactic acid)/halloysite bionanocomposite films. *J. Compos. Mater.* 2014, *48*, 3705–3717.
28. Chen Y., Murphy A., Scholz D., Geever L. M., Lyons J. G., Devine D. M. Surface-modified halloysite nanotubes reinforced poly(lactic acid) for use in biodegradable coronary stents. *J. Appl. Polym. Sci.* 2018, *135*, 46521.
29. Stoclet G., Sclavons M., Lecouvet B., Devaux J., Van Velthem P., Boborodea A., Bourbigota S., Sallem-Idrissi N. Elaboration of poly(lactic acid)/halloysite nanocomposites by means of water assisted extrusion: structure, mechanical properties and fire performance. *RSC Adv.* 2014, *4*, 57553–57563.
30. Guo J., Qiao J., Zhang X. Effect of an alkalized-modified halloysite on PLA crystallization, morphology, mechanical, and thermal properties of PLA/halloysite nanocomposites. *J. Appl. Polym. Sci.* 2016, *133*, 1–9.
31. Fuenmayor E., Forde M., Healy A. V., Devine D. M., Lyons J. G., McConville C., Major I. Material considerations for fused-filament fabrication of solid dosage forms. *Pharmaceutics* 2018, *10*, 1–27.
32. Pinto V. C., Ramos T., Alves S., Xavier J., Tavares P., Moreira P. M. G. P., Guedes R. M. Comparative failure analysis of PLA, PLA/GNP and PLA/CNT-COOH biodegradable nanocomposites thin films. *Procedia Eng.* 2015, *114*, 635–642.
33. Stanković M., Frijlink H. W., Hinrichs W. L. J. Polymeric formulations for drug release prepared by hot melt extrusion: application and characterization. *Drug Discov. Today* 2015, *20*, 812–823.
34. Lyons J. G., Holehonnur H., Devine D. M., Kennedy J. E., Geever L. M., Blackie P., Higginbotham C. L. The incorporation of an organically modified layered silicate in monolithic polymeric matrices produced using hot melt extrusion. *Mater. Chem. Phys.* 2007, *103*, 419–426.
35. Healy A. V., Waldron C., Geever L. M., Devine D. M. Degradable nanocomposites for fused filament fabrication applications. *J. Manuf. Mater. Process.* 2018, *2*, 29.
36. Li Y., Han C., Zhang X., Xu K., Bian J., Poly D. L. (L-lactide)/poly(D-lactide)/clay nanocomposites: enhanced dispersion, crystallization, mechanical properties, and hydrolytic degradation. *Polym. Eng. Sci.* 2014, *54*, 914–924.
37. Sasimowski E., Majewski Ł. Effect of the intensive plasticizing zone design on the effectiveness of corotating twin-screw extrusion. *Adv. Polym. Technol.* 2019, *2019*, 15–17.
38. Albareeki M. M., Driscoll S. B., Barry C. F. Compounding of polyethylene composites using high speed twin and quad screw extruders. *AIP Conf. Proc.* 2019, *2139*, 020006.
39. Atif R., Inam F. Reasons and remedies for the agglomeration of multilayered graphene and carbon nanotubes in polymers. *Beilstein J. Nanotechnol.* 2016, *7*, 1174–1196.
40. Liu M., Zhang Y., Zhou C. Nanocomposites of halloysite and polylactide. *Appl. Clay Sci.* 2013, *75–76*, 52–59.
41. Chen Y., Geever L. M., Killion J. A., Lyons J. G., Higginbotham C. L., Devine D. M. Halloysite nanotube reinforced polylactic acid composite. *Polym. Compos.* 2017, *38*, 2166–2173.
42. Gamon G., Evon P., Rigal L. Twin-screw extrusion impact on natural fibre morphology and material properties in poly(lactic acid) based biocomposites. *Ind. Crop. Prod.* 2013, *46*, 173–185.
43. Normand G., Peuvrel-Disdier E., Vergnes B. Matrix degradation during high speed extrusion of polypropylene/clay nanocomposites – influence on filler dispersion. *Int. Polym. Process.* 2017, *31*, 508–516.
44. Domenech T., Peuvrel-Disdier E., Vergnes B. Influence of twin-screw processing conditions on structure and properties of polypropylene – organoclay nanocomposites. *Int. Polym. Process.* 2012, *27*, 517–526.
45. Villmow T., Kretzschmar B., Pötschke P. Influence of screw configuration, residence time, and specific mechanical energy in twin-screw extrusion of polycaprolactone/multi-walled carbon nanotube composites. *Compos. Sci. Technol.* 2010, *70*, 2045–2055.
46. Wu W., Cao X., Zhang Y., He G. Polylactide/halloysite nanotube nanocomposites: thermal, mechanical properties, and foam processing. *J. Appl. Polym. Sci.* 2013, *130*, 443–452.
47. Prashantha K., Lecouvet B., Sclavons M., Lacrampe M. F., Krawczak P. Poly(lactic acid)/halloysite nanotubes nanocomposites: structure, thermal, and mechanical properties as a function of halloysite treatment. *J. Appl. Polym. Sci.* 2013, *128*, 1895–1903.
48. Devine D. M., Hoctor E., Hayes J. S., Sheehan E., Evans C. H. Extended release of proteins following encapsulation in hydroxyapatite/chitosan composite scaffolds for bone tissue engineering applications. *Mater. Sci. Eng. C* 2017, *84*, 281–289.
49. Yuan Y., Lee R., Bracco G., Holst B. Contact angle and wetting properties. In *Surface Science Techniques*; Springer Series in Surface Sciences, *51*, 2013; pp. 3–34.